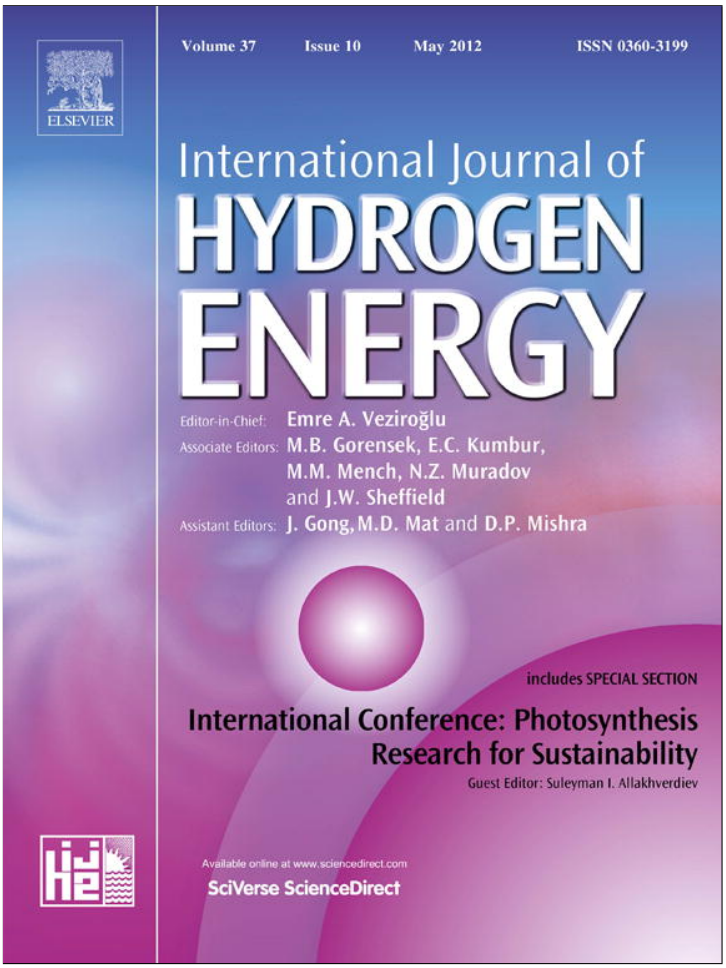

INTERNATIONAL JOURNAL OF HYDROGEN ENERGY 37 (2012) 8505–8511

Available online at www.sciencedirect.com

SciVerse ScienceDirect

journal homepage: www.elsevier.com/locate/he

Technical Communication

Effects of an agglomerate size distribution on the PEFC agglomerate model

*William K. Epting, Shawn Litster**

Department of Mechanical Engineering, Carnegie Mellon University, Scaife Hall 323, 5000 Forbes Ave., Pittsburgh, PA 15213, USA

ARTICLE INFO

Article history:
Received 22 December 2011
Received in revised form
12 February 2012
Accepted 16 February 2012
Available online 20 March 2012

Keywords:
PEFC
Electrode
Agglomerate model
Morphology

ABSTRACT

The agglomerate model of a polymer electrolyte fuel cell (PEFC) electrode typically assumes a single, representative agglomerate diameter, while in reality there is a distribution of agglomerate sizes. Here, we analyze how the agglomerate model's predictions are affected by incorporating an agglomerate diameter distribution. Our analysis shows that the diameter distribution causes the agglomerate model predictions to differ by as much as 70% when compared to even reasonable single agglomerate diameter choices. The error in the model's predictions is highly sensitive to both agglomerate diameter and overpotential. Even the agglomerate diameter that gives the lowest maximum error in our results, 115 nm, errs by as much as 15% at certain overpotentials.

1. Introduction

The agglomerate model for PEFC electrodes [1–16] uses analytical solutions to coupled oxygen diffusion and the reduction reaction in an idealized, spherical agglomerate. It thereby offers a more detailed physical and mathematical description of the transport processes in the electrode compared to the macro-homogeneous or interface approaches [2]. However, most prior implementations of the agglomerate model have assumed a single, representative agglomerate diameter [1–15] (though references [3,7,13] parametrically vary the agglomerate diameter) and do not consider the non-uniform size distributions that actually exist within an electrode. One notable exception is Yoon and Weber [16], who consider a deliberate gradient of agglomerate sizes from the membrane to the diffusion medium. In that approach, the agglomerate size is still a single value across a plane of constant depth. They modeled a hypothetical engineered agglomerate size gradient to examine the possible benefit. In contrast, we consider a size distribution arising from the primary particle aggregate size distribution and uncontrolled agglomeration, and examine how it affects the oxygen reduction reaction (ORR) rates predicted by the agglomerate porous electrode model.

Our recent work [17] used commercial nanoscale X-ray computed tomography (nano-CT) equipment (UltraXRM-L200, Xradia, Inc., Pleasanton, CA) with 50 nm resolution to reconstruct the 3D microstructure of PEFC electrodes (Fig. 1a). The nano-CT imaging distinguished solid agglomerates from secondary pores, but it did not distinguish the individual constituents (e.g. Nafion and Pt/C). The reconstructions were verified using other established characterization techniques,

* *Corresponding author*. Tel.: +1 412 268 3050; fax: +1 412 268 3348.
E-mail address: litster@andrew.cmu.edu (S. Litster).
0360-3199/$ – see front matter
doi:10.1016/j.ijhydene.2012.02.099

which also indicated through comparisons that the segmented solid volume included the Nafion film. In the solid-phase geometry, we fit inscribed spheres to obtain an agglomerate diameter distribution (Fig. 1b).

In the present work, this particular geometry will be incorporated into a simplified agglomerate model to demonstrate the impact of an agglomerate diameter distribution on the total ORR current prediction. In this work, we do not model the performance of an entire fuel cell, nor do we use the model to predict the overall voltage–current behavior. Instead, we consider an idealized volume slice within the electrode (Fig. 2) in which the oxygen concentration in the secondary pores surrounding the agglomerates and the electric potentials are uniform. We thereby focus on the significant difference in predictions incurred by incorporating the agglomerate diameter distribution, when compared to the usual assumption of a single, representative agglomerate size. An advantage of this approach is that it is general. The results we present are relative, not absolute, and they provide a framework for considering agglomerate diameter distributions in a full fuel cell model.

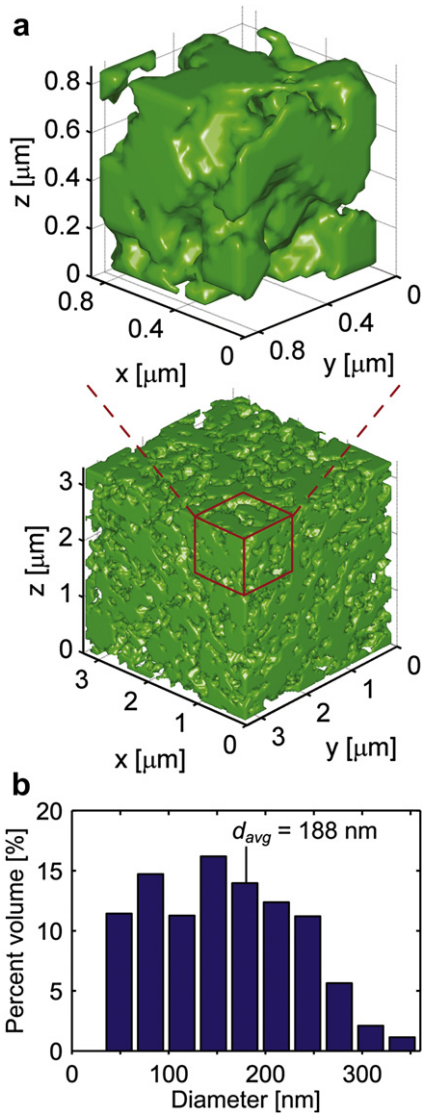

Fig. 1 – Nano-CT characterization of a PEFC electrode's microstructure. a, Nano-CT reconstruction (50 nm resolution) of the solid phase of a PEFC electrode, from Ref. [17]. b, Histogram showing the agglomerate diameter distribution, found by fitting inscribed spheres into the reconstruction shown in image a. The displayed average diameter of 188 nm was computed using volumetric weighting of each agglomerate bin.

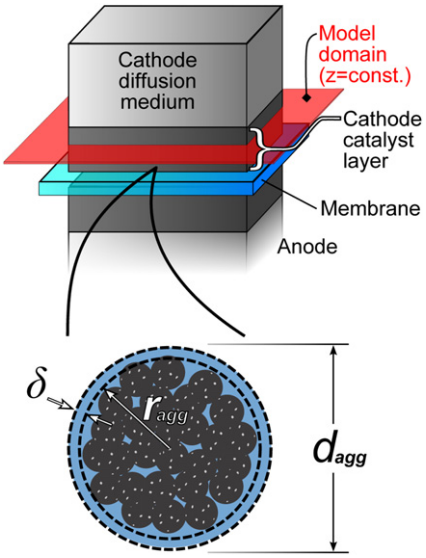

Fig. 2 – Schematic of the model domain. The model presented here considers a small area slice of the catalyst layer at constant depth, in which the gas phase oxygen concentration in the secondary pores and electric potentials are constant. The bottom image depicts nomenclature concerning the spherical agglomerates. Note that the agglomerate diameter includes the ionomer film for comparison to physically measured values, whereas r_{agg} does not, to conform to the method of Thiele [18].

2. Theory

To evaluate the effect of the agglomerate diameter distribution on the predicted reaction rate, we first use the solid-phase diameter distribution in Fig. 1b to estimate a distribution of agglomerate effectiveness factors, drawing on expressions from Sun et al. [1] based on the original work by Thiele [18]. The effectiveness factor represents the reaction rate within an agglomerate divided by the hypothetical reaction rate if transport were infinitely facile. A value close to unity is optimal: this means intra-agglomerate O_2 transport is not hindering the reaction rate. The effectiveness factor is given by

$$E_r = \frac{1}{\Phi_L}\left(\frac{1}{\tanh(3\Phi_L)} - \frac{1}{3\Phi_L}\right) \quad (1)$$

where Thiele's modulus, Φ_L, is given below by Eq. (2), in which r_{agg} represents the radius of the agglomerate up to, but not including, an assumed surrounding ionomer film; k_c is the ORR rate constant (given by Eq. (3)); D is the diffusivity of O_2 in

Nafion®; and ε_{agg} is the agglomerate ionomer fraction, which represents the volume fraction of ionomer within the agglomerate (not including the surrounding ionomer film).

$$\Phi_L = \frac{r_{agg}}{3}\sqrt{\frac{k_c}{D\varepsilon_{agg}^{1.5}}} \tag{2}$$

The ORR rate constant is found from the Butler–Volmer equation as:

$$k_c = \frac{a_{Pt}}{4Ff_{agg}}\frac{i_0}{c_{O_2}^{ref}}\left[\exp\left(\frac{\alpha_c nF\eta_c}{RT}\right) - \exp\left(\frac{-(1-\alpha_c)nF\eta_c}{RT}\right)\right] \tag{3}$$

where a_{Pt} is the electrochemically active volumetric surface area of platinum, F is Faraday's constant, f_{agg} is the electrode's volume fraction of agglomerates not including ionomer film (calculated based on the diameter distribution, the ink composition, a known electrode thickness from TEM, and the assumed thickness δ of the ionomer film), i_0 is the exchange current density, $c_{O_2}^{ref}$ is the reference oxygen concentration associated with i_0, α_c is the cathodic transfer coefficient, n is the number of electrons transferred in the rate limiting step of the reaction, and η_c is the representative local overpotential. We note that recent work has suggested the ORR to have an order less than unity [19]. Yoon and Weber [16] have implemented this finding into an agglomerate model through a numerical model and an approximate correction. However, we assume the common reaction order of 1 for the ORR, which facilitates the exact, analytical solution for the agglomerate model. Also note that k_c is a volumetric parameter for the agglomerate and does not depend on the agglomerate size.

From the distribution of agglomerate effectiveness factors, we calculate a volumetric distribution of reaction rate vs. agglomerate radius. The volumetric reaction rate in an agglomerate is given by:

$$j_{ORR} = 4F\frac{p_{O_2}}{H}\left[\frac{1}{E_r k_c f_{agg}} + \frac{r_{agg}\delta}{a_{agg}D(r_{agg}+\delta)}\right]^{-1} \tag{4}$$

where p_{O_2} is the local partial pressure of oxygen, H is Henry's constant, and a_{agg} is the agglomerate surface area per unit catalyst volume; a_{agg} is taken to be $3f_{agg}/r_{agg}$, which is found from the surface area of a sphere of active material (radius r_{agg}) divided by its volume, scaled by the electrode's volume fraction of the active material in the agglomerate (excludes outer film), f_{agg}. Note that the form of j_{ORR} presented in Eq. (4) differs from Eq. (8) in Sun et al. [1]. We present a derivation in the supplementary material that explains this in more detail. In short, the difference is the inversion of $r_{agg}/(r_{agg}+\delta)$ in the second term. Although Sun et al. use a different form, the inversion of the fraction does not substantially impact the model results for the larger agglomerate sizes they model. The effect is more significant for smaller (order of 100 nm) agglomerates, where the original form results in an unphysical, non-monotonic dependence on diameter. Some of the agglomerates considered in the present work are in that size range.

To understand the effects of the agglomerate size distribution, the quantity we wish to evaluate is the fraction of the total reaction rate carried by each agglomerate diameter, PJ_i. This is done by finding the reaction rate for each agglomerate diameter, weighting it by the volume V_i occupied by agglomerates of that diameter, and dividing it by the total reaction rate for the electrode:

$$PJ_i = \frac{(j_{ORR})_i V_i}{\sum_i [(j_{ORR})_i V_i]} \tag{5}$$

It is important to note that, since j_{ORR} has a linear dependence on p_{O_2} and H in this model, those terms cancel out in this local ratio as shown in Eq. (6).

$$PJ_i = \frac{\cancel{4F\frac{p_{O_2}}{H}}\left[\frac{1}{E_r k_c f_{agg}} + \frac{r_{agg}\delta}{a_{agg}D(r_{agg}+\delta)}\right]_i^{-1} V_i}{\sum_i \left[\cancel{4F\frac{p_{O_2}}{H}}\left[\frac{1}{E_r k_c f_{agg}} + \frac{r_{agg}\delta}{a_{agg}D(r_{agg}+\delta)}\right]_i^{-1} V_i\right]} \tag{6}$$

Since we wish to demonstrate the effect of a non-uniform agglomerate diameter distribution on the model predictions, we consider a simplified system where p_{O_2} is uniform in the gas phase – this could be considered as a small plane of electrode at constant depth within a catalyst layer, as depicted in Fig. 2. Hence, for each current density considered, the gas phase p_{O_2} is the same regardless of the agglomerate size, allowing it to cancel in Eq. (6).

Model parameters are given in Table 1. For the sake of simplicity in this demonstrative model implementation, we made the following further assumptions and generalizations regarding the agglomerate model:

- Because we are considering a planar volume of electrode with a uniform p_{O_2}, the overpotential, η_c is also uniform throughout the electrode plane.

Table 1 – Operating, transport, and electrochemical parameters used in the model.

Description	Value	Unit	Source
T, Temperature	80	°C	[1]
δ, thickness of ionomer film	10	nm	Assumed
ε_{CL}, secondary porosity in catalyst layer	0.43		[17]
ε_{agg}, ionomer fraction in agglomerate	0.22		Calculated
f_{agg}, electrode volume fraction of agglomerates, excluding film	0.34		Calculated
a_{Pt}, electrochemically active Pt surface area	1.04×10^7	m^2_{Pt}/m^3_{CL}	Measurement
α_c, cathodic transfer coefficient	0.61		[1]
i_0, Ref. exchange current density	1.5×10^{-2}	A/m^2	[1]
$c_{O_2}^{ref}$, Ref. O_2 concentration	0.85	mol/m^2	[1]
D, diffusivity of O_2 in Nafion	8.45×10^{-10}	m^2/s	[1]

- The effect of liquid water is not considered. This is in part a consequence of considering relative contributions within an idealized volume of constant p_{O_2}.
- The ionomer film surrounding any agglomerate has a thickness, δ, of 10 nm.
- Excluding the ionomer film surrounding them, all agglomerates were assumed to have identical volumetric composition (i.e. ϵ_{agg} is the same for all agglomerates). The values of 22% and 34% for ϵ_{agg} and f_{agg} were estimated from the nano-CT reconstruction in concert with the assumed value of δ and the known ink composition.
- As in other implementations [1,2,4–13,15,16], the inside of the agglomerate is considered entirely solid material (C, Pt, and ionomer). This is a reasonable simplification: in our recent nano-CT work [17], a comparison between the nano-CT-determined porosity and the expected porosity (calculated from the ink composition and electrode thickness) indicates that the inside of the agglomerates should be roughly 10% porous.
- The volume–average electrochemically active Pt surface area, a_{Pt}, of 1.04×10^7 m^2_{Pt}/m^3_{CL} was calculated using H_2/N_2 cyclic voltammetry performed in our lab on an electrode of composition identical to that of Fig. 1.
- Other physical values are the same as in Ref. [1].

3. Results and discussion

Fig. 3a shows the general effect of agglomerate diameter on the effectiveness factor at three different cathode overpotentials according to Eq. (1). Note that unlike r_{agg} in Eqs. (2) and (4), diameter values reported in this work include the ionomer film (see Fig. 2). The discrepancy is because r_{agg} is a transport length in the particle agglomerate and a model input, whereas the diameter values are for comparison to the measured agglomerate sizes that include the Nafion film. Fig. 3b shows the contribution to the total reaction rate from agglomerates of different diameters, calculated by Eq. (5) in conjunction with each agglomerate diameter's percent volume from Fig. 1b. The overpotentials in these plots of 0.5, 0.6, and 0.7 V were selected to represent a range in which mass transport effects are significant. An important observation of Fig. 3b is that at the lowest overpotential, the reaction rate distribution follows the volumetric distribution of diameter, since all diameters are similarly effective and primarily activation limited. However, at higher overpotentials (and hence higher currents), the smaller agglomerates with their shorter diffusion length scales and consequently higher effectiveness factors contribute to more of the total reaction rate, despite still occupying the same physical volume fraction. Thus, the reaction rate distribution shifts to smaller diameters.

As noted earlier, prior uses of the agglomerate model have assumed a single agglomerate diameter [1–15] or an imposed size gradient [16]. Consequently, a utility of the distribution in Fig. 1b is to extract a single "effective" agglomerate diameter, d_{eff}, that yields equivalent ORR rates to predictions obtained using the agglomerate diameter distributions. In other words, if we assume a single agglomerate diameter, d_{eff}, and implement the agglomerate model, we obtain some overall reaction

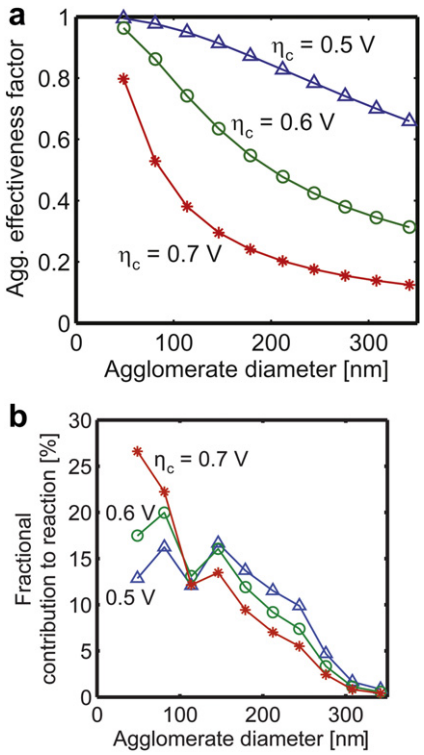

Fig. 3 – The agglomerate diameter and contribution to reaction rate. a, The effect of agglomerate diameter on effectiveness factor at cathode overpotentials of 0.7 V (red squares), 0.6 V (green circles), and 0.5 V (blue triangles). b, Each agglomerate diameter bin's fractional contribution to the overall cathode reaction rate, based on the volumetric distribution of effectiveness factors. (For interpretation of the references to colour in this figure legend, the reader is referred to the web version of this article.)

rate, $j_{tot} = j_{ORR}(d_{eff}, \eta_c)$. Thus, instead of calculating a volume–average or surface-area-average diameter value, we are seeking the value of d_{eff} that yields the same overall reaction rate, j_{tot}, as when we calculate it based on the results from Eqs. (4) and (5) for the measured agglomerate diameter distribution:

$$j_{tot} = \sum_i PJ_i j_{ORR,i} \tag{7}$$

However, since both j_{tot} and each agglomerate-diameter's relative contribution to j_{tot}, PJ_i, depend on overpotential (see Fig. 3b), d_{eff} must also depend on overpotential. Fig. 4a presents the effective diameters calculated from the reaction rate. Note that the range of overpotentials plotted extends from 0.05 V all the way to 1 V. Overpotentials as high as 1 V are not common for PEFC operation, but are relevant nonetheless since they are used in studies of limiting current, which are often used to extract electrode transport parameters [20–25], including estimates of the agglomerate radius [25]. At more common overpotentials near 0.6 V, Fig. 4a still exhibits substantial departure from the low overpotential value. The plot exhibits the strong dependence of the effective diameter, d_{eff}, on the overpotential. The trend toward smaller values of

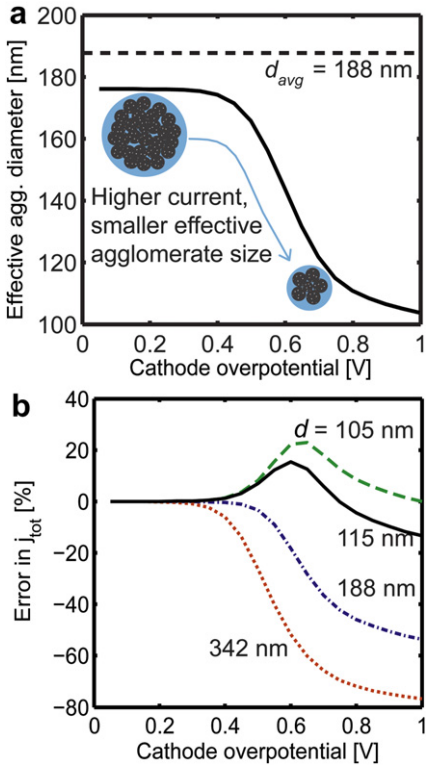

Fig. 4 – Relationship between agglomerate diameter choice and model predictions as a function of overpotential. a, The effective agglomerate diameter, d_{eff}, versus overpotential. The volume–average diameter d_{avg} is shown for comparison. b, For each choice of agglomerate diameter (shown on figure for each curve), the error in j_{tot} when assuming a single agglomerate diameter. The baseline for computing the error is the value found by Equation (7), which accounts for the experimental agglomerate diameter distribution.

d_{eff} at higher overpotentials (higher currents) is consistent with our earlier finding that as overpotential increases, the relative contribution to reaction rate by smaller agglomerates also increases.

The agglomerate diameters shown in Fig. 1b are small compared to the assumed agglomerate diameter in many previous implementations of the agglomerate model [1,2,4,6,7,10–14]. However, the range of sizes used here are in good agreement with prior SAXS [26], TEM [27], and FIB-SEM [28–31] studies. Even assuming a single, smaller diameter like those of Fig. 1b, the errors possible are significant. If the resulting j_{tot} values from Eq. (7) are taken as the "correct" values, we can calculate the error incurred by assuming a single agglomerate diameter as a function of overpotential. Fig. 4b shows these errors in j_{tot} over a range of overpotentials for several different choices of agglomerate diameter.

In Fig. 4b, we display three possible agglomerate diameter choices based on the nano-CT reconstructions: the largest diameter (342 nm), the volume–average diameter (188 nm), and the smallest value of d_{eff} (105 nm) in Fig. 4a. From among these choices, the model can over-predict the reaction rate by as much as 20% and under-predict it by as much as 70%. We also sought the agglomerate diameter that yields the lowest error across the entire range of overpotentials. A choice of 115 nm (±2.5 nm) neither over- nor under-predicted j_{tot} by more than 15%; this choice is also shown in Fig. 4b.

As evident in Fig. 4b, the errors arising from assuming a single agglomerate diameter are highly sensitive to both the assumed agglomerate diameter and the overpotential. This indicates that one should exercise caution when assuming a single agglomerate diameter. However, if one does make this assumption, the analysis presented here suggests that one should assume an agglomerate diameter smaller than the volume average.

4. Conclusions

The agglomerate model of PEFC electrodes typically assumes a single agglomerate diameter when simulating PEFC performance. The primary goal of this work is to demonstrate the importance of an agglomerate size distribution for accurate predictions with an agglomerate model. For this reason, we did not employ a rigorous, full thickness model, as the development and implementation of it would detract from the simpler primary finding. Instead, we used a simplified agglomerate model on a representative elementary volume within the electrode without variations of the gas phase oxygen concentration in the secondary pores or of the electrolyte potential.

Here, we investigated the effect of an agglomerate size distribution using a diameter distribution measured from nano-CT imaging of a typical PEFC electrode. We found a substantial difference between the results of a model that assumes a single agglomerate diameter versus a model that accounts for a size distribution. The error between the agglomerate model with a single diameter and the agglomerate model with a diameter distribution is highly sensitive to both overpotential and the choice of agglomerate diameter. For our particular geometry obtained from nano-CT imaging, we found that an agglomerate diameter of 115 nm yields the lowest error across a broad range of overpotentials, but it still errs by as much as 15%. Although we believe these results are representative, the exact values are not universal and do depend on the size distribution of a particular electrode. In our previous nano-CT measurements, we identified a notable change in the agglomerate size distributions with modest alterations of the electrode preparation procedure.

The results presented here show that a distribution of agglomerate sizes significantly impacts the results of the agglomerate model in an idealized volume where the oxygen concentration is uniform in the surrounding gas pores. In the present work, we do not model the performance of an entire fuel cell. However, to do so is possible using methods similar to those used here to model the ORR for representative elementary volumes in a computational electrode model. As in this work, the oxygen reduction reaction would be binned by the agglomerate size data (as in Fig. 1b), with appropriate parameters extracted from the ink composition, electrode thickness, and an assumed ionomer film thickness. A multi-dimensional model of an entire electrode could employ an approach similar to Eq. (7), incorporating each agglomerate

size bin's contribution to estimate the total reaction rate for each computational node or cell volume. The overall reaction rate can then be used to compute the source/sink terms for each of the governing equations.

Conflict of interest statement

The authors declare no conflicts of interest.

Acknowledgements

The authors gratefully acknowledge the support of the National Science Foundation (NSF) in the award of a Faculty Early Career Development (CAREER) grant for S. Litster, as well as STAR Fellowship Assistance Agreement FP1715401-0, awarded by the U.S. Environmental Protection Agency (EPA) to W. Epting. The EPA has not formally reviewed this publication; the views expressed in it are solely those of the authors, and the EPA does not endorse any products or commercial services mentioned herein. The authors also gratefully acknowledge Prof. Kunal Karan from Queen's University for useful discussions on the agglomerate model, and Jeff Gelb of Xradia, Inc. for his assistance in obtaining the nano-CT data.

Appendix A. Supplementary material

Supplementary material associated with this article can be found, in the online version, at doi:10.1016/j.ijhydene.2012.02.099.

REFERENCES

[1] Sun W, Peppley BA, Karan K. An improved two-dimensional agglomerate cathode model to study the influence of catalyst layer structural parameters. Electrochim Acta 2005;50:3359–74.
[2] Harvey D, Pharoah JG, Karan K. A comparison of different approaches to modelling the PEMFC catalyst layer. J Power Sources 2008;179:209–19.
[3] Xia ZT, Wang QP, Eikerling M, Liu ZS. Effectiveness factor of Pt utilization in cathode catalyst layer of polymer electrolyte fuel cells. Can J Chem 2008;86:657–67.
[4] Secanell M, Karan K, Suleman A, Djilali N. Multi-variable optimization of PEMFC cathodes using an agglomerate model. Electrochim Acta 2007;52:6318–37.
[5] Chang S-M, Chu H-S. Transient behavior of a PEMFC. J Power Sources 2006;161:1161–8.
[6] Khajeh-Hosseini-Dalasm N, Ahadian S, Fushinobu K, Okazaki K, Kawazoe Y. Prediction and analysis of the cathode catalyst layer performance of proton exchange membrane fuel cells using artificial neural network and statistical methods. J Power Sources 2011;196:3750–6.
[7] Obut S, Alper E. Numerical assessment of dependence of polymer electrolyte membrane fuel cell performance on cathode catalyst layer parameters. J Power Sources 2011;196:1920–31.
[8] Shah AA, Kim GS, Gervais W, Young A, Promislow K, Li J, et al. The effects of water and microstructure on the performance of polymer electrolyte fuel cells. J Power Sources 2006;160:1251–68.
[9] Sousa T, Mamlouk M, Scott K. An isothermal model of a laboratory intermediate temperature fuel cell using PBI doped phosphoric acid membranes. Chem Eng Sci 2010;65:2513–30.
[10] Siegel NP, Ellis MW, Nelson DJ, von Spakovsky MR. Single domain PEMFC model based on agglomerate catalyst geometry. J Power Sources 2003;115:81–9.
[11] Broka K, Ekdunge P. Modelling the PEM fuel cell cathode. J Appl Electrochem 1997;27:281–9.
[12] Jaouen F, Lindbergh G, Sundholm G. Investigation of mass-transport limitations in the solid polymer fuel cell cathode. J Electrochem Soc 2002;149:A437–47.
[13] Gloaguen F, Durand R. Simulations of PEFC cathodes: an effectiveness factor approach. J Appl Electrochem 1997;27:1029–35.
[14] Das PK, Li X, Liu Z-S. A three-dimensional agglomerate model for the cathode catalyst layer of PEM fuel cells. J Power Sources 2008;179:186–99.
[15] Perry ML, Newman J, Cairns EJ. Mass transport in gas-diffusion electrodes: a diagnostic tool for fuel-cell cathodes. J Electrochem Soc 1998;145:5–15.
[16] Yoon W, Weber AZ. Modeling low-platinum-loading effects in fuel-cell catalyst layers. J Electrochem Soc 2011;158:B1007–18.
[17] Epting WK, Gelb J, Litster S. Resolving the three-dimensional microstructure of polymer electrolyte fuel cell electrodes using nanometer-scale X-ray computed tomography. Adv Funct Mater 2012;22:555–60.
[18] Thiele EW. Relation between catalytic activity and size of particle. Ind Eng Chem 1939;31:916–20.
[19] Neyerlin KC, Gu W, Jorne J, Gasteiger HA. Determination of catalyst unique parameters for the oxygen reduction reaction in a PEMFC. J Electrochem Soc 2006;153:A1955–63.
[20] Williams MV, Kunz HR, Fenton JM. Analysis of polarization curves to evaluate polarization sources in hydrogen/air PEM fuel cells. J Electrochem Soc 2005;152:A635–44.
[21] St-Pierre J, Wetton B, Kim GS, Promislow K. Limiting current operation of proton exchange membrane fuel cells. J Electrochem Soc 2007;154:B186–93.
[22] Beuscher U. Experimental method to determine the mass transport resistance of a polymer electrolyte fuel cell. J Electrochem Soc 2006;153:A1788–93.
[23] Baker DR, Caulk DA, Neyerlin KC, Murphy MW. Measurement of oxygen transport resistance in PEM fuel cells by limiting current methods. J Electrochem Soc 2009;156:B991–1003.
[24] Sambandam S, Ramani V. Influence of binder properties on kinetic and transport processes in polymer electrolyte fuel cell electrodes. Phys Chem Chem Phys 2010;12:6140–9.
[25] Kudo K, Suzuki T, Morimoto Y. Analysis of oxygen dissolution rate from gas phase into Nafion surface and development of an agglomerate model. ECS Trans 2010;33:1495–502.
[26] Xu F, Zhang HY, Ilavsky J, Stanciu L, Ho D, Justice MJ, et al. Investigation of a catalyst ink dispersion using both ultra-small-angle X-ray scattering and cryogenic TEM. Langmuir 2011;26:19199–208.
[27] Xie J, Wood DL, More KL, Atanassov P, Borup RL. Microstructural changes of membrane electrode assemblies during PEFC durability testing at high humidity conditions. J Electrochem Soc 2005;152:A1011–20.

[28] Zils S, Timpel M, Arlt T, Wolz A, Manke I, Roth C. 3D visualisation of PEMFC electrode structures using FIB nanotomography. Fuel Cells 2010;10:966–72.
[29] Ziegler C, Thiele S, Zengerle R. Direct three-dimensional reconstruction of a nanoporous catalyst layer for a polymer electrolyte fuel cell. J Power Sources 2011;196:2094–7.
[30] Kuroda CS, Yamazaki Y. Novel technique of MEA sample preparation using a focused ion beam for scanning electron microscope investigation. ECS Trans 2007;11:509–16.
[31] Schulenburg H, Schwanitz B, Krbanjevic J, Linse N, Mokso R, Stampanoni M, et al. 3D imaging of polymer electrolyte fuel cell electrodes. ECS Trans 2010;33:1471–81.